

Ergoregion instability of exotic compact objects: Electromagnetic and gravitational perturbations and the role of absorption

Elisa Maggio,^{1,2,3} Vitor Cardoso,^{2,4} Sam R. Dolan,¹ and Paolo Pani³

¹*Consortium for Fundamental Physics, School of Mathematics and Statistics,*

University of Sheffield, Hicks Building, Hounsfield Road, Sheffield S3 7RH, United Kingdom

²*Centro de Astrofísica e Gravitação—CENTRA, Departamento de Física, Instituto Superior Técnico—IST,*

Universidade de Lisboa—UL, Avenida Rovisco Pais 1, 1049-001 Lisboa, Portugal

³*Dipartimento di Fisica, “Sapienza” Università di Roma & Sezione INFN Roma 1,*

Piazzale Aldo Moro 5, 00185 Roma, Italy

⁴*Perimeter Institute for Theoretical Physics, 31 Caroline Street North Waterloo,*

Ontario N2L 2Y5, Canada



(Received 30 July 2018; published 8 March 2019)

Spinning horizonless compact objects may be unstable against an “ergoregion instability.” We investigate this mechanism for electromagnetic perturbations of ultracompact Kerr-like objects with a reflecting surface, extending previous (numerical and analytical) work limited to the scalar case. We derive an analytical result for the frequency and the instability timescale of unstable modes which is valid at small frequencies. We argue that our analysis can be directly extended to gravitational perturbations of exotic compact objects in the black-hole limit. The instability for electromagnetic and gravitational perturbations is generically stronger than in the scalar case, and it requires larger absorption to be quenched. We argue that exotic compact objects with spin $\chi \lesssim 0.7$ ($\chi \lesssim 0.9$) should have an absorption coefficient of at least 0.3% (6%) to remain linearly stable, and that an absorption coefficient of at least $\approx 60\%$ would quench the instability for any spin. We also show that—in the static limit—the scalar, electromagnetic, and gravitational perturbations of the Kerr metric are related to one another through Darboux transformations. Finally, correcting previous results, we give the transformations that bring the Teukolsky equation in a form described by a real potential also in the gravitational case.

DOI: [10.1103/PhysRevD.99.064007](https://doi.org/10.1103/PhysRevD.99.064007)

I. INTRODUCTION

Exotic compact objects (ECOs) are under intense scrutiny as probes of near-horizon quantum structures [1–3], as models for exotic states of matter in ultracompact stars [4], and even as exotic gravitational-wave (GW) sources that might coexist in the Universe along with black holes (BHs) and neutron stars as in certain dark-matter scenarios (see Refs. [2,3,5] for recent overviews).

The phenomenology of ECOs depends strongly on their compactness (or, equivalently, on the gravitational redshift z at their surface). Objects with $z \sim \mathcal{O}(1)$ (e.g., boson stars [6,7]) have properties similar to those of neutron stars and display $\mathcal{O}(1)$ corrections in most observables (e.g., multipole moments [8–11], geodesic motion [12], quasinormal mode (QNM) ringing [13–16], tidal Love numbers [17–19], etc.) relative to BHs.

A different class of ECOs (dubbed *ClePhOs* in the terminology introduced in Refs. [2,3]) is instead associated with modifications of the Kerr metric only very close to the horizon, as in some quantum-gravity scenarios [20–27]. Here, then, $z \sim \mathcal{O}(10^{20})$ or larger for objects with mass

$M \sim 10 M_{\odot}$ or higher. It is extremely challenging—if not impossible [2,3,28]—to rule out or detect these objects through electromagnetic observations, since their geodesic structure is almost identical to that of a BH. On the other hand, GWs emitted by these objects in different scenarios carry unique information on their properties. This includes (i) GW echoes in the postmerger ringdown phase of a binary coalescence [1,18] (see also Ref. [29] for an earlier study, and Refs. [30–35] for a debate on the evidence of this effect in aLIGO data); (ii) a (logarithmically small) tidal deformability that affects the late inspiral [36,37]; (iii) the absence of tidal heating for ECOs as compared to BHs [37]; (iv) their different spin-induced quadrupole moment [9–11,38]; and (v) the stochastic GW background from a population of ECOs [39–41].

In parallel with developing detection strategies for these signatures, it is also important to assess the viability of ECOs and, in particular, their stability and their formation channels. Spinning ECOs are potentially unstable, due to the so-called *ergoregion instability* [42] (for a review, see Ref. [43]). The latter is an instability that develops in any

asymptotically flat spacetime featuring an ergoregion but without an event horizon: since physical negative-energy states can exist inside the ergoregion—a key ingredient in Penrose’s process [44]—it is energetically favorable to cascade toward even more negative states. The only way to prevent such a process from developing is by absorbing the negative-energy states. Kerr BHs can absorb radiation very efficiently and are indeed stable even if they have an ergoregion. On the other hand, compact horizonless geometries are generically unstable in the absence of dissipation mechanisms.

The ergoregion instability has been studied for various models [42,43,45–51]. The timescale of the instability depends strongly on the spin and on the compactness of the object [43,49,52]. In particular, the instability exists only for those objects which are compact enough to possess a photon sphere [43,53]. The latter is naturally present in all models of ECOs that modify the BH geometry only at the horizon scale, for example by invoking an effective surface located at some Planck distance from the would-be horizon [2,3].

The ergoregion instability of Planck-inspired ECOs has been recently studied in Ref. [54] for scalar-field perturbations. There, it was shown that, if the ECO interior does not absorb any radiation, the instability timescale is short enough to have a crucial impact on the dynamics of the object. On the other hand, partial absorption (i.e., reflectivity at the object’s surface smaller than unity) may quench the instability completely, just like in the BH case. Because the dissipation of energy in compact objects made of known matter is small, the instability imposes severe constraints on some particular models of horizonless objects [40].

In this paper we extend the analysis of Ref. [54] to electromagnetic and gravitational perturbations. Since the ergoregion instability is intimately linked to superradiance [43,55], and since superradiance is enhanced by field spin (at least for rapidly spinning objects), one expects that the instability gets stronger for gravitational perturbations. Below, we quantify this expectation—both by solving the full linear problem numerically and by computing the spectrum of unstable modes analytically in the small-frequency limit—and we discuss the implications of our results for current observational constraints on ECOs.

Any instability is, of course, also related to the boundary conditions of the problem. While formulating physical boundary conditions for electromagnetic and gravitational fluctuations, we uncovered a curious relation between all sets of perturbations in the static limit: scalar, electromagnetic, and gravitational perturbations of the Kerr metric are all related to one another through Darboux transformations. To the best of our knowledge, this interesting property of BH perturbations in general relativity has not been reported before. Through this work, we use $G = c = 1$ units.

II. SETUP

A. Kerr-like ECO model

Our setup and methods follow Refs. [40,54]. We consider a geometry described by the Kerr metric¹ when $r > r_0$ and, at $r = r_0$, we assume the presence of a membrane with some reflective properties. Different models of ECOs are characterized by different properties of the membrane at $r = r_0$, in particular by a (possibly) frequency-dependent reflectivity [54,59]. In Boyer-Lindquist coordinates, the line element at $r > r_0$ reads

$$ds^2 = -\left(1 - \frac{2Mr}{\Sigma}\right)dt^2 + \frac{\Sigma}{\Delta}dr^2 - \frac{4Mr}{\Sigma}a\sin^2\theta d\phi dt + \Sigma d\theta^2 + \left[(r^2 + a^2)\sin^2\theta + \frac{2Mr}{\Sigma}a^2\sin^4\theta\right]d\phi^2, \quad (1)$$

where $\Sigma = r^2 + a^2 \cos^2\theta$ and $\Delta = r^2 + a^2 - 2Mr$, with M and $J := aM$ being the total mass and spin of the object.

Motivated by models of microscopic corrections at the horizon scale, in the following we shall focus on the case

$$r_0 = r_+(1 + \epsilon) \quad 0 < \epsilon \ll 1, \quad (2)$$

where $r_+ = M + \sqrt{M^2 - a^2}$ is the location of the would-be horizon. Although the above parametrization requires $a \leq M$, the latter condition is not strictly necessary [54]; the case of so-called “superspinars” (when $a > M$ [50,51,54,62]) will be discussed elsewhere. Note that ϵ is related to the compactness of the object and to the gravitational redshift at the surface, namely $M/r_0 \approx M/r_+(1 + \epsilon)$ and $z \approx \epsilon^{-1/2}(r_+/M - 1)^{-1/2}$. If $r_0 \sim r_+ + l_P$ (where l_P is the Planck length, as suggested by some quantum-gravity-inspired models [1–3]), then $\epsilon \sim 10^{-40}$ for a nonspinning object with $M \sim 50 M_\odot$.

B. Linear perturbations

Scalar, electromagnetic, and gravitational perturbations in the exterior Kerr geometry are described in terms of Teukolsky’s master equations [63–65]:

¹The vacuum region outside a spinning object is not necessarily described by the Kerr geometry, due to the absence of an analog to Birkhoff’s theorem in axisymmetry. This implies that the multipolar structure of a spinning ECO might be generically different from that of a Kerr BH. However, in those models that admit a smooth BH limit, there are indications that all multipole moments of the external spacetime approach those of a Kerr BH as $\epsilon \rightarrow 0$ [9–11,56–58]. In fact, for $z \rightarrow \infty$, it is natural to expect that the exterior spacetime is extremely close to Kerr, unless some discontinuity occurs in the BH limit. See Refs. [30,40,54,59–61] for other work discussing the same model.

$$\Delta^{-s} \frac{d}{dr} \left(\Delta^{s+1} \frac{d_s R_{lm}}{dr} \right) + \left[\frac{K^2 - 2is(r-M)K}{\Delta} + 4is\omega r - \lambda \right] {}_s R_{lm} = 0, \quad (3)$$

$$[(1-x^2)_s S_{lm,x}]_x + \left[(a\omega x)^2 - 2a\omega s x + s + {}_s A_{lm} - \frac{(m+sx)^2}{1-x^2} \right] {}_s S_{lm} = 0, \quad (4)$$

where ${}_s S_{lm}(\theta) e^{im\phi}$ are spin-weighted spheroidal harmonics, $x \equiv \cos \theta$, $K = (r^2 + a^2)\omega - am$, and the separation constants λ and ${}_s A_{lm}$ are related by $\lambda \equiv {}_s A_{lm} + a^2\omega^2 - 2am\omega$. When $a = 0$, the angular eigenvalues are $\lambda = (l-s)(l+s+1)$, whereas for $a \neq 0$ they can be computed numerically or with approximated analytical expansions (see Sec. II D below).

It is convenient to make a change of variables by introducing Detweiler's function [66]

$${}_s X_{lm} = \Delta^{s/2} (r^2 + a^2)^{1/2} \left[\alpha {}_s R_{lm} + \beta \Delta^{s+1} \frac{d_s R_{lm}}{dr} \right], \quad (5)$$

where α and β are certain radial functions. Introducing the tortoise coordinate r_* , defined such that $dr_*/dr = (r^2 + a^2)/\Delta$, the master equation (3) becomes

$$\frac{d_s^2 X_{lm}}{dr_*^2} - V(r, \omega) {}_s X_{lm} = 0, \quad (6)$$

where the effective potential is

$$V(r, \omega) = \frac{U\Delta}{(r^2 + a^2)^2} + G^2 + \frac{dG}{dr_*}, \quad (7)$$

and

$$G = \frac{s(r-M)}{r^2 + a^2} + \frac{r\Delta}{(r^2 + a^2)^2}, \quad (8)$$

$$U = V_s + \frac{2\alpha' + (\beta' \Delta^{s+1})'}{\beta \Delta^s}, \quad (9)$$

$$V_s = -\frac{1}{\Delta} [K^2 - is\Delta'K + \Delta(2isK' - \lambda)]. \quad (10)$$

The prime denotes a derivative with respect to r , and the functions α and β can be chosen such that the resulting potential is purely real (see Ref. [66] for the definitions of α and β in the electromagnetic case and Appendix B for the gravitational case).² In the following, we define $R_s \equiv {}_s R_{lm}$, $X_s \equiv {}_s X_{lm}$, and omit the l, m subscripts for brevity.

²Reference [66] has some mistakes in the definitions of the radial functions α and β in the gravitational case, which we correct in Appendix B.

C. Boundary conditions

By imposing boundary conditions at infinity and at the surface of the ECO, Eq. (6) defines an eigenvalue problem whose eigenvalues, $\omega = \omega_R + i\omega_I$, are the QNMs of the system. In our convention a stable mode corresponds to $\omega_I < 0$, whereas an unstable mode corresponds to $\omega_I > 0$ with the instability timescale $\tau := 1/\omega_I$.

In order to derive the QNM spectrum, we impose outgoing boundary conditions at infinity [65]:

$$X_s \sim e^{i\omega r_*}, \quad r \rightarrow \infty. \quad (11)$$

At $r = r_0$, there is a superposition of ingoing and outgoing waves. In general, the boundary condition depends on the properties of the membrane of the ECO. In the following, we will mainly focus on the analysis of a perfectly reflecting surface—a discussion about the role of partial absorption by the object is presented in Sec. VI. In the case of electromagnetic perturbations, we consider a perfect conductor in which the electric and magnetic fields satisfy $E_\theta(r_0) = E_\phi(r_0) = 0$ and $B_r(r_0) = 0$. By writing the previous conditions in terms of the three complex scalars of the electromagnetic field in the Newman-Penrose formalism [67], we obtain the following boundary conditions on Teukolsky's function [43]:

$$\partial_r R_{-1} = \left[\frac{iK}{\Delta} - \frac{i}{2K} (\lambda \pm B + 2i\omega r) \right] R_{-1}, \quad (12)$$

where³ $B = \sqrt{\lambda^2 + 4ma\omega - 4a^2\omega^2}$, and the plus and minus signs refer to polar and axial perturbations, respectively. Note that the above boundary conditions define a perfectly conducting object, since the outgoing energy flux is equal to the incoming flux at the surface. In Sec. III A, we will show that the boundary conditions in Eq. (12) are equivalent to the following boundary conditions on Dirichlet's function, when $\epsilon \ll 1$:

$$\begin{cases} X_{-1}(r_0) = 0 & \text{axial} \\ dX_{-1}(r_0)/dr_* = 0 & \text{polar} \end{cases} \quad (13)$$

Motivated by a ‘‘bounce and amplify’’ argument (see Sec. V A below), we shall extend this result to gravitational perturbations of a perfectly reflecting ECO, in which case we impose

$$\begin{cases} X_{-2}(r_0) = 0 & \text{axial} \\ dX_{-2}(r_0)/dr_* = 0 & \text{polar} \end{cases} \quad (14)$$

³We notice that Ref. [43] has a typo in the definition of B .

D. Numerical procedure

Equation (6) with the boundary conditions (11) and (12) [or (13) and (14)] can be solved numerically through a direct integration shooting method [68]. Starting with a high-order series expansion at large distances, we integrate Eq. (6) [or, equivalently, Eq. (3)] from infinity to $r = r_0$; we repeat the integration for different values of ω until the desired boundary condition at r_0 is satisfied.

The QNMs of the system depend on two continuous dimensionless parameters: the spin $\chi = a/M$ and the parameter ϵ , defined in Eq. (2), that is related to the ECO compactness and to the redshift at the ECO surface. Furthermore, the QNMs depend on three integer numbers: the angular number $l \geq 0$, the azimuthal number m (such that $|m| \leq l$), and the overtone number $n \geq 0$. We shall focus on the fundamental modes ($n = 0$) with $l = m = 1$ for electromagnetic perturbations and $l = m = 2$ for gravitational perturbations which, in the unstable case, correspond to the modes with the largest imaginary part, and thus the shortest instability timescale. In our numerical results, we also make use of the symmetry [69]

$$m \rightarrow -m, \quad \omega_R \rightarrow -\omega_R, \quad {}_sA_{lm} \rightarrow {}_sA_{l-m}^*. \quad (15)$$

The latter guarantees that, without loss of generality, we can focus on modes with $m \geq 0$ only.

Finally, the angular eigenvalues can be computed numerically using continued fractions [70]. For $a\omega \ll 1$, ${}_sA_{lm}$ can also be expanded analytically as ${}_sA_{lm} = \sum_{n=0} f_{slm}^{(n)} (a\omega)^n$, where $f_{slm}^{(n)}$ are known expansion coefficients [70]. The above expression provides an excellent approximation whenever $|a\omega| \lesssim 1$. In the numerical results presented below, we have used the full numerical expression of ${}_sA_{lm}$ obtained through continued fractions. We checked that the analytical approximation (up to second order) differs from exact eigenvalues by $\lesssim 2\%$ for the electromagnetic modes at high spin and by $\lesssim 4\%$ for the gravitational modes.

III. ECO INSTABILITIES FOR ELECTROMAGNETIC PERTURBATIONS

A. Analytical results: Extension of Vilenkin's calculation to electromagnetic perturbations

Here we extend Vilenkin's analytical computation [45] of scalar perturbations in the background of a perfectly reflecting Kerr-like object to the electromagnetic case. We use Detweiler's transformation [Eq. (5)] and introduce standard "in" and "up" modes, denoted X_s^+ and X_s^- , respectively, with asymptotic behavior

$$X_s^+ \sim \begin{cases} B_+ e^{-i\tilde{\omega}r_*} & r_* \rightarrow -\infty \\ e^{-i\omega r_*} + A_+ e^{+i\omega r_*} & r_* \rightarrow \infty \end{cases}, \quad (16a)$$

$$X_s^- \sim \begin{cases} e^{+i\tilde{\omega}r_*} + A_- e^{-i\tilde{\omega}r_*} & r_* \rightarrow -\infty \\ B_- e^{+i\omega r_*} & r_* \rightarrow \infty \end{cases}, \quad (16b)$$

where $\tilde{\omega} = \omega - m\Omega$ and $\Omega = a/(2Mr_+)$ is the angular velocity at the horizon. Since the effective potential in Eq. (6) is real, X_s^\pm and their complex conjugates $X_s^{\pm*}$ are independent solutions to the same equation which satisfy complex conjugated boundary conditions. Via the Wronskian relationships, the coefficients A_\pm and B_\pm satisfy the relations [71]

$$1 - |A_+|^2 = (\tilde{\omega}/\omega)|B_+|^2, \quad (17a)$$

$$1 - |A_-|^2 = (\omega/\tilde{\omega})|B_-|^2, \quad (17b)$$

and $\tilde{\omega}B_+ = \omega B_-$, from which it follows that $|A_-| = |A_+|$.

We focus on the solution with asymptotics [Eq. (16b)], and we impose the boundary conditions [Eq. (12)] at the surface; i.e., we assume that the latter is a perfect conductor. Near the surface, the function R_{-1} defined in Eq. (12) has the following asymptotics:

$$R_{-1}^- \sim \mathcal{A} \Delta e^{-i\tilde{\omega}r_*} + \mathcal{B} e^{+i\tilde{\omega}r_*} \quad r_* \rightarrow -\infty, \quad (18)$$

where $\mathcal{A} = \mathcal{A}_0 + \eta \mathcal{A}_1 + \dots$ and $\mathcal{B} = \mathcal{B}_0 + \eta \mathcal{B}_1 + \dots$, with $\eta \equiv r - r_+$. Since $\Delta \sim (r_+ - r_-)\eta$ near the surface, in Eq. (18) we consider $\mathcal{A} = \mathcal{A}_0$ and $\mathcal{B} = \mathcal{B}_0 + \eta \mathcal{B}_1$. We then obtain

$$\mathcal{B}_0 = \frac{-2^{1/2}(r_+^2 + a^2)^{1/2} \tilde{\omega}}{B}, \quad (19)$$

$$\mathcal{A}_0 = \frac{-iB}{4K_+ \mathfrak{R}^*} \mathcal{B}_0 A_-, \quad (20)$$

where $K_+ = K(r_+)$, $\mathfrak{R} = iK_+ + (r_+ - r_-)/2$ [71]. By inserting Eq. (18) in the Teukolsky equation, we find

$$\mathcal{B}_1 = \left(\frac{iam}{M(r_+ - r_-)} + \frac{2\omega r_+ - i\lambda}{4Mr_+ \tilde{\omega}} \right) \mathcal{B}_0. \quad (21)$$

Equation (18) with Eqs. (19)–(21) defines the asymptotic expansion of R_{-1} near the horizon at the first order in η . By inserting Eq. (18) in the boundary condition [Eq. (12)], we get the following expression:

$$e^{i\tilde{\omega}r_*^0} \mp A_- e^{-i\tilde{\omega}r_*^0} = 0 \quad (22)$$

for the two signs of Eq. (12), respectively, which correspond to polar (−) and axial (+) modes, and where $r_*^0 = r_*(r_0)$. The above equation takes the same form as Eq. (11) in Ref. [45] for scalar perturbations. Note that Eq. (22) implies that the perfect-conductor boundary conditions [Eq. (12)] correspond to the Dirichlet and Neumann boundary conditions on the function X_{-1}^- for

axial and polar modes, respectively [see above Eq. (13) for an explicit expression]. Equation (22) yields

$$\tilde{\omega} = \frac{1}{2|r_*^0|} (p\pi - \Phi + i \ln |A_-|), \quad (23)$$

where p is a positive odd (even) integer for axial (polar) modes and Φ is the phase of the reflected wave at $r = r_0$.

In order to compute the imaginary part of the mode, we first recall that $|A_-| = |A_+|$, so we need to derive $|A_+|$. For waves originating at infinity, the “in” mode X_{-1}^+ has asymptotics [Eq. (16a)]. If we express the latter in terms of Teukolsky’s function R_{-1} , we find

$$R_{-1}^+ \sim r^{-1} \mathcal{C} e^{-i\omega r_*} + r \mathcal{D} e^{i\omega r_*} \quad r_* \rightarrow \infty, \quad (24)$$

where the coefficients of incident and reflected waves are $\mathcal{C} = 1/(2^{3/2}|\omega|)$ and $\mathcal{D} = \frac{4\omega^2}{B} \mathcal{C} A_+$ [71]. In the electromagnetic case the amplification factor is defined as [43]

$$Z = \frac{|\mathcal{D}|^2}{|\mathcal{C}|^2} \frac{B^2}{16\omega^4} - 1, \quad (25)$$

which implies

$$Z = |A_+|^2 - 1. \quad (26)$$

In the low-frequency regime, the amplification coefficient for generic spin- s waves in the Kerr metric has been computed by Starobinsky [72]:

$$Z = -D_{lm} = 4Q\beta_{sl} \prod_{k=1}^l \left(1 + \frac{4Q^2}{k^2} \right) [\omega(r_+ - r_-)]^{2l+1}, \quad (27)$$

where $\sqrt{\beta_{sl}} = \frac{(l-s)!(l+s)!}{(2l)!(2l+1)!}$ and $Q = \frac{r_+^2 + a^2}{r_+ - r_-} (m\Omega - \omega)$. In our calculations we consider $Z = -\text{Re}\{D_{lm}\}$, since the QNM frequency is complex and $\omega_I \ll \omega_R$.

By inserting Eq. (27) into Eq. (26) and recalling that $|A_+| = |A_-|$, we derive the imaginary part of the frequency in Eq. (23):

$$|A_-|^2 - 1 = -\text{Re}\{D_{lm}\}, \quad (28)$$

which is analogous to the Vilenkin relation for scalar perturbations. Note that $Z > 0$ (i.e., $\omega_I > 0$) in the super-radiant regime $\omega_R(\omega_R - m\Omega) < 0$. We have therefore shown that electromagnetic unstable modes of a perfectly reflecting Kerr-like object can be understood in terms of waves being amplified at the ergoregion and reflected at the boundary.

In Appendix A, we derive an analogous result using a matched asymptotic expansion. In addition, the latter allows us to compute the phase Φ in Eq. (23) analytically.

To summarize, the analytical result valid at small frequency reads⁴

$$\omega_R \sim -\frac{\pi}{2|r_*^0|} \left[q + \frac{s(s+1)}{2} \right] + m\Omega, \quad (29)$$

$$\omega_I \sim -\frac{\beta_{sl}}{|r_*^0|} \left(\frac{2Mr_+}{r_+ - r_-} \right) [\omega_R(r_+ - r_-)]^{2l+1} (\omega_R - m\Omega), \quad (30)$$

where $r_*^0 \sim M[1 + (1 - \chi^2)^{-1/2}] \log \epsilon$ and q is a positive odd (even) integer for polar (axial) modes. The above result is valid for $s = -1$, for $s = 0$ [in the latter case, q is a positive odd (even) integer for Neumann (Dirichlet) boundary conditions on the scalar field], and also for gravitational perturbations when $s = -2$; the latter result will be discussed in Sec. V. Furthermore, we note that the hypothesis of low frequency implies that $M\omega_R \ll 1$. In order to fulfill this condition in the spinning case, it is not sufficient that $\log \epsilon \ll 1$, but also that $M\Omega \ll 1$. Indeed, in the BH limit ($\epsilon \rightarrow 0$) we obtain $\omega_R \sim m\Omega$ (hence, the frequency is independent on ϵ as long as $\Omega M \gg \epsilon$) and $\omega_I \sim (m\Omega)^{2l+1} / \log^2 \epsilon$. In this limit, the above analytical result is strictly valid only when $\Omega M \ll 1$.

On the other hand, the analytical result is always accurate near the critical value of the spin such that $\omega_R \approx 0$ and $\omega_I \approx 0$. The above equations predict that the instability occurs when $\omega_R(\omega_R - m\Omega) < 0$, which, for $\epsilon \rightarrow 0$, implies (for $s = -1$)

$$\chi > \chi_{\text{crit}} \approx \frac{\pi q}{m |\log \epsilon|}. \quad (31)$$

Therefore, the critical value of the spin above which the instability occurs can be very small as $\epsilon \rightarrow 0$. However, in the same limit the instability timescale is $\tau \propto \log^2 \epsilon / (m\Omega)^{2l+1}$ [54]. In other words, as $\epsilon \rightarrow 0$, also slowly spinning ECOs become unstable. In the same limit, their instability timescale can be very long but still relevant on dynamical scales [54].

B. Numerical results

Figure 1 shows the agreement between the QNMs computed numerically and analytically through a matched asymptotic expansion. As expected, the agreement is very good in the small-frequency regime, i.e., when both $\log \epsilon$ and ΩM are small. In particular, the agreement is excellent near the critical value of the spin χ_{crit} (since $\omega = 0$ at the

⁴Comparison between Eqs. (29) and (23) reveals that the phase Φ defined in Eq. (23) is a constant and does not depend on the spin. This analytical result is in contrast with the phase computed numerically in Ref. [54]. Since the phase is computed from a matched asymptotic expansion, we believe that the spin dependence of Φ computed in Ref. [54] is due to a different approximation in the calculation. Indeed, in the region near the surface of the ECO, Eq. (A3) of Ref. [54] neglects more terms proportional to $a\omega$ with respect to Eq. (A1).

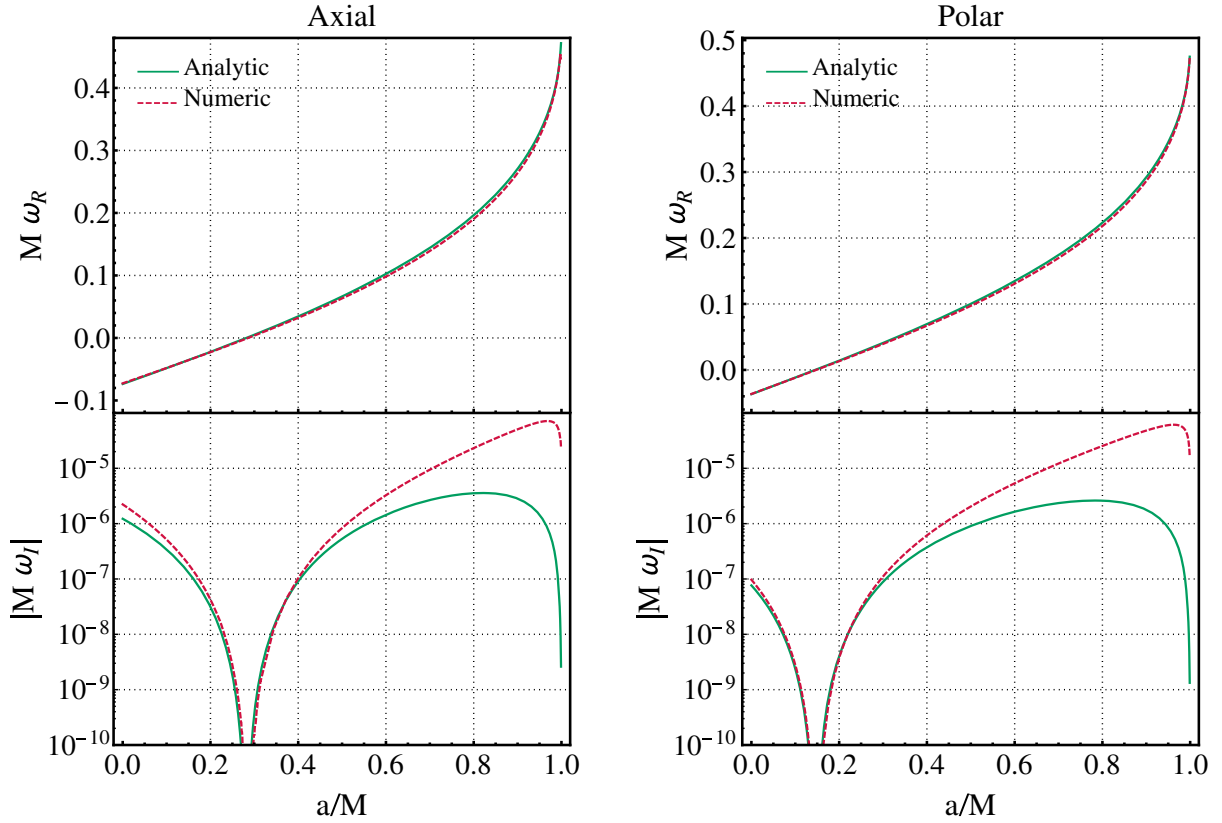


FIG. 1. Real (top panels) and imaginary (bottom panels) parts of the fundamental electromagnetic QNM ($l = m = 1, n = 0$) of an ECO as a function of the spin. The left (right) panels refer to axial (polar) modes [corresponding to a minus (plus) sign in Eq. (12)]. The surface of the ECO is located at $r_0 = r_+(1 + \epsilon)$ with $\epsilon = 10^{-10}$. The QNMs computed numerically (dashed curves) are in agreement with the QNMs computed analytically through Eqs. (29) and (30) (continuous curves) when $M\omega \ll 1$. The cusps in the imaginary part of the frequency correspond to the threshold of the ergoregion instability, above which the QNMs turn from stable to unstable. Note that the instability is still present in the extremal Kerr case ($a = M$) and continuously matches the instability of superspinars ($a > M$) [50,51,54,62]. The analytical approximation breaks down in the high-spin regime, since $\omega_R M \sim m\Omega M \approx m/2$ is not small.

critical value). When $a \approx 0$, the agreement improves as $\epsilon \rightarrow 0$, since in such limit, $\omega \rightarrow 0$. On the other hand, when $a \approx M$, $M\omega \rightarrow mM\Omega \approx m/2$ as $\epsilon \rightarrow 0$, and therefore finite-frequency effects become important, especially for $m > 1$.

Notice that for both axial and polar modes, the imaginary part of the frequency changes sign for a critical value of the spin; i.e., for $a > a_{\text{crit}}$ the ECO model becomes unstable against the ergoregion instability. The instability is still present in the extremal Kerr case ($a = M$) and in the superspinar case ($a > M$). When $a = M$, the QNMs computed analytically are not reliable—since they are not in the small-frequency regime—thus we can rely only on the numerical results in order to estimate the instability in the extremal Kerr case. The instability in the superspinar case will be discussed in detail in a separate work.

An interesting feature is that the threshold of instability is the same for both scalar and electromagnetic perturbations within our numerical accuracy, as shown in the right panel of Fig. 2. In particular, scalar modes with Dirichlet (Neumann) boundary conditions on Teukolsky's function R_0 turn unstable for the same critical value of the spin of

electromagnetic axial (polar) modes. In the next section, we explain this finding analytically in terms of Darboux transformations [73] between perturbations of the Kerr metric with different s indices.

In the left panel of Fig. 2, we notice that the real part of scalar QNMs with Dirichlet (Neumann) boundary conditions and that of electromagnetic axial (polar) QNMs tends to be the same in the BH limit, $\epsilon \rightarrow 0$. This remark is confirmed by the analytical description of QNMs given in Eq. (29). According to the latter, the real part of the frequency is the same for $s = 0$ and $s = -1$, and $\omega_R \sim m\Omega$ for $\epsilon \ll 1$ and any value of s .

Moreover, as shown in the right panel of Fig. 2, the imaginary part of the frequency displays a similar trend for scalar Dirichlet (Neumann) QNMs and electromagnetic axial (polar) QNMs. The numerics is in agreement with Eq. (30), according to which the imaginary part of the frequency in the electromagnetic case is the same as the scalar one multiplied by a factor β_{11}/β_{01} .

We also notice that the electromagnetic axial and polar modes tend to be the same in the BH limit, as it happens for

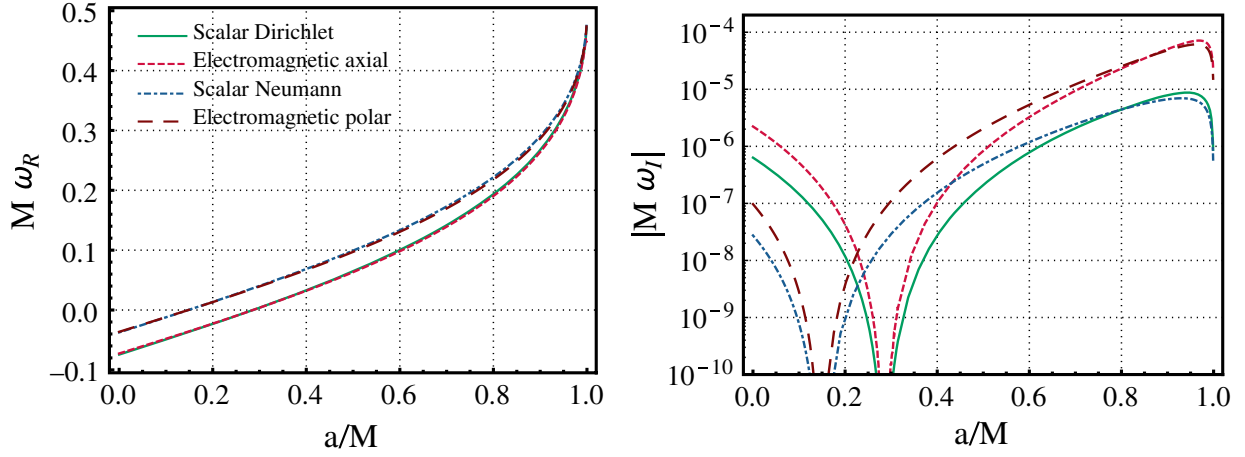


FIG. 2. Real (left panel) and imaginary (right panel) parts of the fundamental scalar and electromagnetic QNMs of an ECO as a function of the spin, where the surface of the ECO is at $r_0 = r_+(1 + \epsilon)$ with $\epsilon = 10^{-10}$. The cusps in the imaginary part of the frequency are the threshold of the ergoregion instability, above which the QNMs becomes unstable. The scalar QNMs with Dirichlet (Neumann) boundary conditions show a correspondence with the electromagnetic axial (polar) QNMs: the real part of the frequency tends to be the same for $\epsilon \ll 1$, and the critical value of instability is identical (within our numerical accuracy).

the scalar QNMs with Dirichlet and Neumann boundary conditions in the same limit [54]. This feature can be understood analytically by noticing that, as $\epsilon \rightarrow 0$, Eq. (12) reduces to

$$\frac{dR_{-1}}{dr_*} = i\tilde{\omega}R_{-1} \quad (32)$$

for both axial and polar modes. Therefore, in the BH limit, axial and polar electromagnetic modes of the ECO are isospectral. Given that this is the case for a BH [74], it is natural to conjecture that isospectrality in the BH limit is a generic feature for any type of perturbation.

IV. STATIC MODES AND DARBOUX TRANSFORMATIONS

The zero-frequency modes are associated with the onset of the ergoregion instability [43,54] for reflecting boundary conditions. Here we seek a relationship between ϵ , the compactness parameter, and a_{crit} , the critical value of the spin at which the instability appears.

For $\omega = 0$, Teukolsky's equation (3) reduces to the radial equation

$$\Delta^{-s} \frac{d}{dr} \left(\Delta^{s+1} \frac{dR_s}{dr} \right) + \left(\frac{a^2 m^2 + 2is(r-M)am}{\Delta} - \lambda \right) R_s = 0, \quad (33)$$

where $\lambda = (l-s)(l+s+1)$.

A. Zero-frequency modes: Scalar field

For $s = 0$, Eq. (33) has the general solution

$$R_0 = c_P P_l^{i\nu}(2x+1) + c_Q Q_l^{i\nu}(2x+1), \quad (34)$$

where $\nu \equiv 2am/(r_+ - r_-)$ and $x \equiv (r - r_+)/(r_+ - r_-)$. Here $P_l^{i\nu}(\cdot)$ and $Q_l^{i\nu}(\cdot)$ are associated Legendre functions with the branch cut along the real axis from $-\infty$ to 1. The boundary condition of regularity as $r \rightarrow \infty$ imposes that $c_P = 0$. At the surface $r = r_0$, we impose totally reflecting (Dirichlet or Neumann) boundary conditions. That is,

$$Q_l^{i\nu}(1+2x_0) = 0 \quad \text{or} \quad \left. \frac{d}{dx} Q_l^{i\nu}(1+2x) \right|_{x=x_0} = 0, \quad (35)$$

where $x_0 = \epsilon r_+/(r_+ - r_-)$. By solving Eq. (35) numerically, we obtain the relationship between ϵ and the value of a for which a static mode occurs.

For ultracompact objects characterized by $\epsilon \ll 1$, it is appropriate to use

$$Q_l^{i\nu} \approx \frac{e^{-\pi\nu}}{2\Gamma(i\nu)} \left[x^{-i\nu/2} + \frac{\Gamma(-i\nu)\Gamma(l+1+i\nu)}{\Gamma(i\nu)\Gamma(l+1-i\nu)} x^{i\nu/2} \right], \quad (36)$$

leading to

$$\ln \frac{\epsilon r_+}{r_+ - r_-} \approx -\frac{\pi(p+1)}{\nu} + \frac{i}{\nu} \ln \frac{\Gamma(1-i\nu)\Gamma(l+1+i\nu)}{\Gamma(1+i\nu)\Gamma(l+1-i\nu)}, \quad (37)$$

where p is a non-negative even (odd) integer for Neumann (Dirichlet) modes. This makes it straightforward to find the relationship between $\ln \epsilon$ and $\nu = 2a_{\text{crit}}m/(r_+ - r_-)$, and thus a_{crit} , the critical value of a at the threshold of the ergoregion instability.

Figure 3 shows the zero-frequency modes in the $(\epsilon, a_{\text{crit}})$ domain, for the Neumann (p even) and Dirichlet (p odd) boundary conditions, for the $l = m$ modes with $m = 1$ (solid lines), $m = 2$ (dashed) and $m = 3$ (dotted). The plot shows that the ergoregion instability afflicts corotating modes of the field. For each $m > 0$, there is a minimum

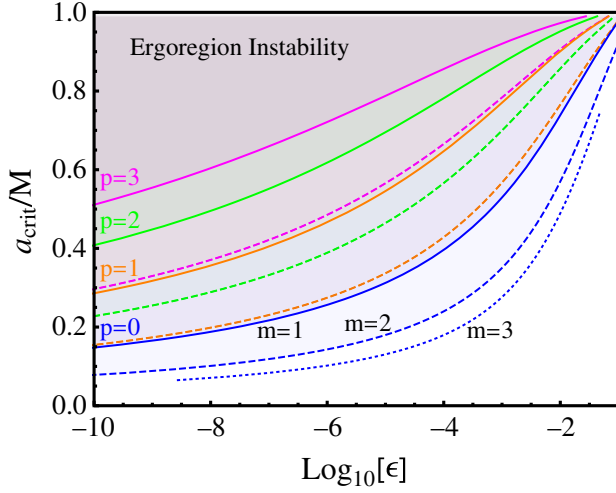


FIG. 3. The ergoregion instability in the ECO spin-compactness parameter space. The lines show the zero-frequency scalar QNMs in the $(\epsilon, a_{\text{crit}})$ domain with Neumann (p even) and Dirichlet (p odd) boundary conditions on the ECO surface at $r_0 = r_+(1 + \epsilon)$. The solid, dashed, and dotted lines show the $m = 1, 2,$ and 3 modes with $l = m$, respectively. The shaded regions indicate where the corresponding modes suffer the ergoregion instability.

value a_{crit} below which the mode is stable. Let us notice that a_{crit} decreases as m increases, and as ϵ decreases, so that even slowly rotating ECOs can suffer an ergoregion instability [54], in principle. (For highly spinning ECOs, see Refs. [75,76].)

In the limit $a \rightarrow 0$ and $\epsilon \rightarrow 0$, Eq. (37) reduces to

$$a_{\text{crit}} \approx \frac{\pi(p+1)}{m|\log \epsilon|} M, \quad (38)$$

which is analogous to Eq. (31) derived analytically in the small-frequency regime. So, for example, a totally reflecting barrier at the Planck scale outside the horizon of a $10 M_{\odot}$ BH ($\epsilon = l_p/r_+ \sim 5 \times 10^{-40}$) will generate an ergoregion instability in the dipole mode ($m = 1$) if $a \gtrsim 0.035$.

B. Darboux transformations

Now, let us consider electromagnetic and gravitational perturbations. It is straightforward to verify that, for $\omega = 0$, the radial functions R_s are related to one another through the following transformations:

$$R_{-1} = R_0 + \frac{i\Delta}{am} R'_0, \quad (39a)$$

$$R_{-2} = \frac{2a^2m^2 - l(l+1)\Delta - 2iam(r-M)}{am(2am - i(r_+ - r_-))} R_0 + \frac{2\Delta(iam + r - M)}{am(2am - i(r_+ - r_-))} R'_0, \quad (39b)$$

defined up to multiplication by a constant factor. Though this relation is not unique, it seems to be the unique transformation for which the fields are regular at large distances. Equivalent transformations are

$$R_0 = -\frac{iam}{l(l+1)} \left[R'_{-1} + \frac{iam}{\Delta} R_{-1} \right], \quad (40a)$$

$$R_{-2} = \frac{am - 2i(r-M)}{2am - i(r_+ - r_-)} R_{-1} + \frac{i\Delta}{2am - i(r_+ - r_-)} R'_{-1}. \quad (40b)$$

C. Zero-frequency modes: Electromagnetic and gravitational perturbations

In the zero-frequency limit, the boundary condition (12) on the electromagnetic wave function, reduces to

$$R'_{-1} + i \left(\frac{am}{\Delta} - \frac{\zeta_{\pm} l(l+1)}{am} \right) R_{-1} = 0, \quad (41)$$

where $\zeta_+ = 1$ for polar modes and $\zeta_- = 0$ for axial modes. By comparison with Eq. (40a), we see that axial modes are generated from a scalar-field solution with a Dirichlet boundary condition $R_0(r_0) = 0$. For the polar modes, we may take a derivative of Eq. (40a) and use the static Teukolsky equation (33) to establish that

$$\Delta R'_0 = \frac{a^2m^2}{l(l+1)} \left[R'_{-1} + i \left(\frac{am}{\Delta} - \frac{l(l+1)}{am} \right) R_{-1} \right]. \quad (42)$$

Thus, from Eq. (41), the polar modes are generated from a scalar-field solution with a Neumann boundary condition⁵ $R'_0(r_0) = 0$. It is natural to posit that this extends to gravitational perturbations as well, in which case one has the following boundary conditions in the zero-frequency limit:

$$R'_{-2} = - \left[\frac{(l-1)(l+2)}{2(iam + r - M)} + \frac{iam}{\Delta} \right] R_{-2}, \quad (43a)$$

$$R'_{-2} = - \frac{iam(l-1)(l+2)}{2iam(iam + r - M) + l(l+1)\Delta} R_{-2} - \frac{iam}{\Delta} R_{-2}, \quad (43b)$$

which are generated from a scalar-field solution with Dirichlet and Neumann boundary conditions, respectively.

By virtue of the Darboux transformations, it follows that Eqs. (35) and (37) and Fig. 3 fully describe the

⁵In Ref. [54], the Neumann boundary condition is imposed on the radial wave function Y_0 , defined as $Y_0 = (r^2 + a^2)^{1/2} R_0$. However, in the small- ϵ limit, the QNM spectrum is analogous to the spectrum obtained by imposing a Neumann boundary condition on R_0 .

zero-frequency modes of not just a scalar field, but also electromagnetic perturbations for an object with perfectly reflecting boundary conditions. [Note, however, that the critical spin is slightly different in the gravitational case, as discussed in the next section; see Eq. (46).]

To the best of our knowledge, these properties of static perturbations of the Kerr metric have not been presented before. In particular, the above relations show that the $\omega \rightarrow 0$ limit of generic spin- s perturbations is universal.

V. ECO INSTABILITIES FOR GRAVITATIONAL PERTURBATIONS

In principle, gravitational perturbations of our Kerr-like ECO model can be studied by solving Teukolsky's equation (3) [or its alternative version in Detweiler's form (6)] with $s = \pm 2$. However, in this case the issue of boundary conditions is much more subtle (see Ref. [77] for a related discussion). In the electromagnetic case, the boundary conditions (12) are derived by assuming that the object is made of a conducting material, so that the two boundary conditions in Eq. (12) are ultimately related to the requirement that the electric and magnetic field be orthogonal and parallel to the surface, respectively [43]. An analog equation for the gravitational case is currently not available. Furthermore, in analogy with the electromagnetic case, the boundary condition must depend on the properties of the object's surface, which are also unknown and generically model dependent.

Nevertheless, we now argue that the results of the previous section can be easily extended to the gravitational case when $\epsilon \rightarrow 0$, at least if the object is perfectly reflecting.

A. Analytical results

The previous analytical computation for the electromagnetic case can be easily understood from a ‘‘bounce and amplify’’ argument [3,43], i.e., in terms of quasistanding waves of a reflecting cavity between the surface of the ECO and the photon sphere. Then the waves slowly leak out through tunneling in the photon-sphere barrier. The frequency of (corotating) modes is set by the width of the cavity, i.e., $\omega_R - m\Omega \sim \pi/r_*^0$, whereas the instability is controlled by the amplification factor Z of the ergoregion at this frequency [43], i.e., $\omega_I \sim Z\omega_R$. A right-moving wave originating at the horizon has the asymptotics given by Eq. (16b). When it is backscattered by the photon-sphere, it acquires a factor A_- , where $|A_-| = |A_+|$ due to the Wronskian relationships (17a) and (17b). After this, the left-moving wave is further reflected at the surface of the ECO and is backscattered at the photon sphere again. At each following bounce at the photon sphere, it acquires a factor A_- . In turn, the factor A_+ describes the backscattering of a wave originating at infinity [Eq. (16b)] and is related to the superradiant amplification factor of BHs through Eq. (26). Thus, at each bounce the wave is

amplified by a factor Z . This argument applies to perfectly reflecting compact objects, since in this case the energy is conserved near the surface during subsequent bounces.

A more quantitative way to look at this effect is to notice that the boundary conditions in Eq. (12) reduce to Dirichlet and Neumann boundary conditions for the Detweiler function X_s^- . As we have shown, this is true for both scalar ($s = 0$) and electromagnetic ($s = \pm 1$) perturbations. It is now natural to conjecture that the same is true for gravitational perturbations, namely that Dirichlet and Neumann conditions on $X_{\pm 2}^-$ imply perfect reflection at the surface (i.e., no absorption by the interior). With this working assumption, the analytical derivation of Sec. III A follows straightforwardly, and the final result in Eqs. (29) and (30) is valid also for low-frequency gravitational perturbations ($s = \pm 2$), the only difference being due to the phase of ω_R computed in Sec. II of Appendix A, namely

$$\omega_R \sim -\frac{\pi(q+1)}{2|r_*^0|} + m\Omega, \quad (44)$$

$$\omega_I \sim -\frac{\beta_{2l}}{|r_*^0|} \left(\frac{2Mr_+}{r_+ - r_-} \right) [\omega_R(r_+ - r_-)]^{2l+1} (\omega_R - m\Omega), \quad (45)$$

where q is a positive odd (even) integer for polar (axial) modes. Note that the above result is a particular case of Eqs. (29) and (30) for $s = -2$. In particular, in the gravitational case, the real part of the frequency has a factor π of difference in the phase compared to the scalar and electromagnetic cases.

Equation (44) implies that the gravitational modes become unstable for a critical value of the spin, which is different from the electromagnetic case, in particular (for $s = -2$):

$$\chi > \chi_{\text{crit}} \approx \frac{\pi(q+1)}{m|\log \epsilon|}. \quad (46)$$

For example, for $\epsilon = 10^{-10}$ and $l = m = 2$, $\chi_{\text{crit,em}} \approx 0.14$, whereas $\chi_{\text{crit,grav}} \approx 0.20$ for axial modes, and $\chi_{\text{crit,em}} \approx 0.07$, whereas $\chi_{\text{crit,grav}} \approx 0.14$ for polar modes.

Furthermore, in the $\epsilon \rightarrow 0$ limit ($\omega_R \rightarrow m\Omega$), the instability timescale is proportional to the inverse of the term $\beta_{sl}[m\Omega(r_+ - r_-)]^{2l+1}[q + s(s+1)/2]$ in ω_I . Since $\beta_{11} = 4\beta_{01}$, the instability timescale for electromagnetic perturbations is simply 4 times shorter than for scalar perturbations. On the other hand, for gravitational perturbations the dominant mode has $|s| = l = m = 2$, which gives $\beta_{22} = \beta_{11}/25$. Taking into account also the $[m\Omega(r_+ - r_-)]^{2l+1}[q + s(s+1)/2]$ term, in the $\epsilon \rightarrow 0$ limit we obtain

$$\tau_{222} = \frac{25(1 + \sqrt{1 - \chi^2})^2 q}{32\chi^2(1 - \chi^2)(1 + q)} \tau_{111}, \quad (47)$$

where $\tau_{slm} = 1/\omega_I$ for a given (s, l, m) . Note that $\tau_{222} > \tau_{111}$ for any spin, showing that the dominant ($l=2$) gravitational instability is actually *weaker* than the dominant ($l=1$) electromagnetic instability in the low-frequency limit. This is consistent with the fact that the amplification factor for $s=l=2$ waves is smaller than that of $s=l=1$ waves at low frequency [43] (see also Fig. 5 below).

Finally, our conjecture is also supported by the zero-frequency limit discussed in Sec. IV, where we showed that the behavior for scalar, electromagnetic, and gravitational perturbations is universal in the zero-frequency limit. Indeed, the boundary conditions in Eq. (14) respectively reduce to Eq. (43) for $\omega \rightarrow 0$ (which also requires $a \rightarrow a_{\text{crit}}$) and $\epsilon \rightarrow 0$.

B. Numerical results

We solve Teukolsky's equation (3) for gravitational perturbations numerically by assuming Dirichlet and Neumann boundary conditions for Detweiler's function X_{-2} [see Eqs. (14)]. A representative example is shown in Fig. 4, where we present the fundamental ($n=0$) $l=m=2$

gravitational modes of an ECO as a function of the spin. The qualitative behavior of the modes is very similar to the electromagnetic case (compare Fig. 4 with Fig. 1), and the agreement with the analytical result derived in the previous section is very good in the regime where $M\omega \ll 1$, i.e., near the threshold of the instability.

Note that in this case the frequency is overall larger, since $\omega_R M \rightarrow 2\Omega M \approx 1$ for $m=2$ and $\chi \rightarrow 1$. In this limit, the quantity $a\omega \approx 1$ and the angular eigenvalues need to be computed numerically.

VI. DISCUSSION: THE ROLE OF ABSORPTION AND ASTROPHYSICAL IMPLICATIONS

Owing to the logarithmic dependence in Eq. (30), the ergoregion instability timescale for perfectly reflecting ECOs is always very short, even for Planck-inspired objects with $\epsilon \sim \mathcal{O}(10^{-40})$ [54]. The most natural development of the instability is to remove angular momentum until the superradiant condition is saturated [53]. Thus, spin measurements of dark compact objects indirectly rule out perfectly reflecting ECOs. Furthermore, the absence of any detectable gravitational-wave stochastic background in

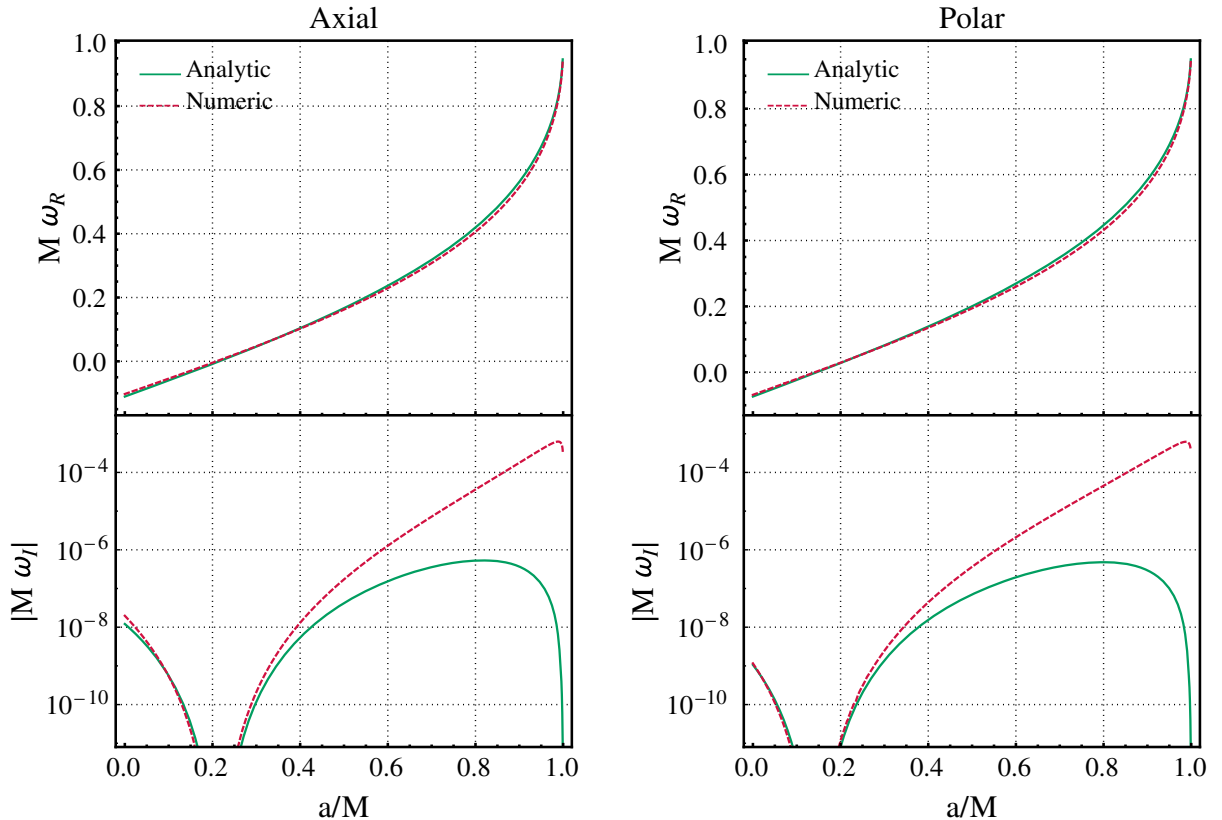


FIG. 4. Real (top panels) and imaginary (bottom panels) parts of the fundamental gravitational QNM ($l=m=2, n=0$) of an ECO as a function of the spin. The left (right) panels refer to axial (polar) modes corresponding to Dirichlet (Neumann) boundary conditions on Detweiler's function X_{-2} , and the surface of the ECO is at $r_0 = r_+(1 + \epsilon)$, with $\epsilon = 10^{-10}$. The QNMs computed numerically (dashed curves) are in agreement with the QNMs computed analytically through Eqs. (44) and (45) (continuous curves) when $M\omega \ll 1$. In the extremal Kerr case ($a=M$), the analytical approximation is not valid, since $M\omega = \mathcal{O}(1)$.

LIGO O1 [78,79] sets the most stringent constraints to date on these models [40]. (It is worth mentioning that the stochastic gravitational-wave background specifically from the spin-down of remnants of binary mergers is not inconsistent with gravitational wave observations, as discussed in Ref. [41].)

However, the instability can be totally quenched by (partial) absorption by the object interior [54]. In the case of scalar perturbations, this requires reflectivity $\sim 0.4\%$ smaller than unity [54]. This number corresponds to the maximum superradiant amplification factor for scalar perturbations of a Kerr BH [43,80], and it is indeed consistent with the “bounce and amplify” argument presented in the previous section. Namely, from Eq. (16b) a right-moving monochromatic wave is backscattered by the ECO potential and acquires a factor $A_- = A_+$. The reflected wave travels to the left and is further reflected at the surface. Let us assume that the reflection coefficient (i.e., the ratio between the outgoing energy flux and the ingoing energy flux) at the object’s surface is $|\mathcal{R}(\omega)|^2$. Then, the left-moving wave $A_+ e^{-i\omega r_*}$ is reflected at the surface as $A_+ \mathcal{R} e^{i\omega r_*}$ (see Ref. [81] for a model based on geometrical optics and Ref. [59] for a generic discussion). The process continues indefinitely, and the wave acquires a factor $A_+ \mathcal{R}$ for each bounce. Therefore, the condition for the energy in the cavity to grow indefinitely in time is $|A_+ \mathcal{R}|^2 > 1$ or

$$|\mathcal{R}|^2 > \frac{1}{1+Z}, \quad (48)$$

where both the amplification factor $Z = |A_+|^2 - 1$ and the ECO reflection coefficient $|\mathcal{R}|^2$ are evaluated at the dominant frequency $\omega = \omega_R$. In the low-frequency regime, Z is approximately given by Eq. (27), but it can be computed numerically for any frequency and spin [43,65]. Since $|\mathcal{R}|^2 \leq 1$, Eq. (48) implies that a necessary condition for the instability is $Z > 0$; i.e., the relevant frequency needs to be in the superradiant regime to trigger the instability. Furthermore, if the object is perfectly reflecting ($|\mathcal{R}|^2 = 1$), the instability is quenched only when $Z < 0$, i.e., only in the absence of superradiance. Likewise, if the object is almost a BH ($\mathcal{R} \approx 0$), the instability is absent for any finite amplification factor Z .

Equation (48) also implies that, in order to quench the instability completely, it is sufficient that $|\mathcal{R}|^2 > 1/(1+Z_{\max}) \approx 1 - Z_{\max}$, where Z_{\max} is the maximum amplification coefficient,⁶ and the last approximation is valid when $Z_{\max} \ll 1$, as is typically the case [43,65].

The above discussion is consistent with the analysis of Ref. [54] for scalar perturbations, but it is actually valid for any kind of perturbations of our ECO model in the BH limit. In general, Eq. (48) implies that the larger the BH

⁶A less stringent condition is $|\mathcal{R}(\omega_R)|^2 > 1/(1+Z(\omega_R))$, where ω_R is the dominant QNM frequency.

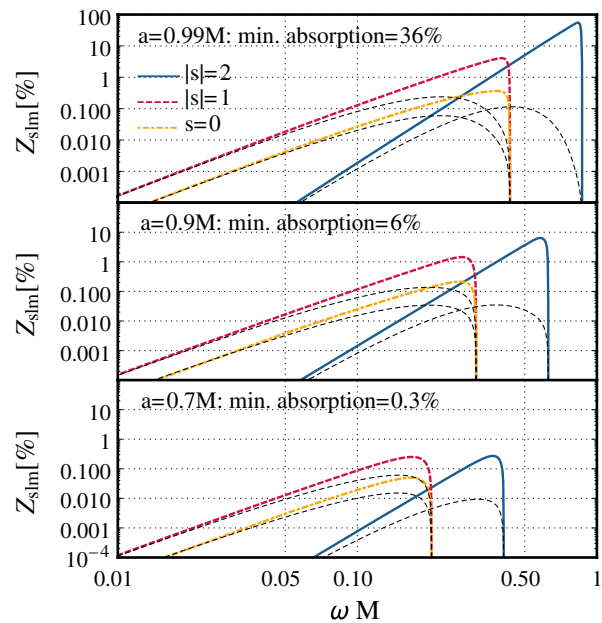


FIG. 5. Superradiant amplification factor for a Kerr BH as a function of the frequency ω of the incident wave for different values of the BH spin and for different types of perturbations (we set $l = m = 1$ for scalar and electromagnetic perturbations, and $l = m = 2$ for gravitational perturbations). The analytical approximation [Eq. (27)] valid at low frequency (black dashed lines) is compared to the exact numerical result [43,65]. In each panel, we report the minimum absorption coefficient at the ECO surface, $1 - |\mathcal{R}|^2$, necessary to quench the instability, as obtained by saturating Eq. (48).

amplification factor, the larger is the minimum absorption rate necessary to quench the instability. The superradiant amplification factor (and hence the minimum absorption rate required to quench the instability) depends significantly on the spin. This is shown in Fig. 5, where we present $Z(\omega)$ for different values of the spin of a Kerr BH and for different types of perturbations [43,65]. As predicted by the analytical result, electromagnetic perturbations have the largest amplification factor at low frequency. On the other hand, gravitational perturbations can be amplified much more than electromagnetic or scalar perturbations at high frequency, which by the superradiant condition $\omega(\omega - m\Omega)$ also requires highly spinning objects. The minimum absorption coefficient, $1 - |\mathcal{R}|^2$, required to quench the instability depends strongly on the spin. For an ECO spinning at $\chi \lesssim 0.9$ ($\chi \lesssim 0.7$), an absorption coefficient of at least 6% (0.3%) is sufficient to quench the instability for any type of perturbation. On the other hand, since the maximum superradiance amplification factor is $\approx 138\%$ (for $l = m = 2$ gravitational perturbations of almost extremal BHs [43,65]), Eq. (48) predicts that an absorption coefficient of at least $\approx 60\%$ would quench the instability in *any* case.

In other words, if a specific ECO can be parametrized by an absorption coefficient of (say) $\approx 1\%$ and it is rapidly

spinning when produced (say, $\chi \approx 1$), it would lose angular momentum over a short timescale given by the ergoregion instability, until it reached a critical value of the spin corresponding to the saturation of Eq. (48). From Fig. 5, in this example the saturation would roughly correspond to a final spin $\chi \approx 0.8$.

VII. CONCLUSION

We have computed the ergoregion instability for electromagnetic and gravitational perturbations of a model of Kerr-like ECO, both numerically (for any compactness and spin) and analytically (in the low-frequency regime, which is valid for small spin and in the BH limit). These cases are qualitatively similar to the scalar case studied in Ref. [54] and allow us to draw a general picture of the ergoregion instability for ECOs. In particular, we showed the following: (i) Our analytical result can also be extended to the gravitational perturbations of a perfectly reflecting ECOs in the BH limit. (ii) The instability can be understood in terms of waves trapped within the photon-sphere barrier and amplified by superradiant scattering [43]. Therefore, for any kind of perturbations, the instability is completely quenched if the absorption rate at the ECO surface is at least equal to the maximum superradiance amplification for a given spin- s perturbation of a Kerr BH with the same mass and spin. (iii) The numerical results for both electromagnetic and gravitational perturbations agree well with the analytical ones in the small-frequency approximation.

As a byproduct of our analysis, we have also found a set of Darboux transformations that relate the waveforms of $s = 0, \pm 1, \pm 2$ perturbations of the Kerr metric in the static limit. It would be interesting to check whether similar transformations exist also between bosonic and fermionic ($s = \pm 1/2$) perturbations. For the latter, there is no superradiance [43], and therefore even highly spinning, perfectly reflecting ECOs should be stable against $s = \pm 1/2$ perturbations.

An interesting extension concerns superspinars, i.e., string-inspired, regularized Kerr geometries spinning above the Kerr bound [62]. The ergoregion instability of these models has been studied for scalar perturbations [50,54] and for gravitational ones [50,51]. However, in the latter case, the boundary conditions adopted do not correspond to Dirichlet or Neumann conditions on the Detweiler function, which, as we argued in this work, are the appropriate ones for gravitational perturbations. In light of our results, it would be interesting to extend the stability analysis of superspinars, both for perfectly reflecting and for partially absorbing models.

ACKNOWLEDGMENTS

We thank Swetha Bhagwat for interesting discussions. The authors acknowledge networking support by the COST Action No. CA16104. V.C. acknowledges financial

support provided under the European Union's H2020 ERC Consolidator Grant "Matter and strong-field gravity: New frontiers in Einstein's theory," Grant Agreement No. MaGRaTh-646597. P.P. acknowledges the financial support provided under the European Union's H2020 ERC, Starting Grant Agreement No. DarkGRA-757480, and the kind hospitality of the Universitat de les Illes Balears, where this work has been finalized. S.D. acknowledges financial support from the European Union's Horizon 2020 research and innovation programme under the H2020-MSCA-RISE-2017 Grant No. FunFiCO-777740, and from the Science and Technology Facilities Council (STFC) under Grant No. ST/P000800/1. E. M. and P. P. acknowledge support from the Amaldi Research Center funded by the MIUR program "Dipartimento di Eccellenza" (CUP: B81I18001170001).

APPENDIX A: ANALYTICAL ASYMPTOTIC MATCHING FOR SPIN- s PERTURBATIONS

In this appendix, we derive the electromagnetic and gravitational QNMs of an ECO analytically in the small-frequency regime through a matched asymptotic expansion.

In the region near the surface of the ECO, the radial wave equation (3) reduces to [72]

$$[x(x+1)]^{1-s} \partial_x \{ [x(x+1)]^{s+1} \partial_x R_s \} + [Q^2 + iQs(1+2x) - \lambda x(x+1)] R_s = 0, \quad (\text{A1})$$

where $x = (r - r_+)/ (r_+ - r_-)$, $Q = (r_+^2 + a^2)(m\Omega - \omega) / (r_+ - r_-)$, and $\lambda = (l-s)(l+s+1)$. Equation (A1) is valid when $M\omega \ll 1$, and it is derived by neglecting the terms proportional to ω in Eq. (3) except for the ones which enter into Q . The general solution of Eq. (A1) is a linear combination of hypergeometric functions:

$$R_s = (1+x)^{iQ} [C_1 x^{-iQ} {}_2F_1(-l+s, l+1+s; 1-\bar{Q}+s; -x) + C_2 x^{iQ-s} {}_2F_1(-l+\bar{Q}, l+1+\bar{Q}; 1+\bar{Q}-s; -x)], \quad (\text{A2})$$

where $\bar{Q} = 2iQ$. The large- r behavior of the solution is

$$R_s \sim \left(\frac{r}{r_+ - r_-} \right)^{l-s} \Gamma(2l+1) \left[\frac{C_1 \Gamma(1-\bar{Q}+s)}{\Gamma(l+1-\bar{Q})\Gamma(l+1+s)} + \frac{C_2 \Gamma(1+\bar{Q}-s)}{\Gamma(l+1+\bar{Q})\Gamma(l+1-s)} \right] + \left(\frac{r}{r_+ - r_-} \right)^{-l-1-s} \times \frac{(-1)^{l+1+s}}{2\Gamma(2l+2)} \left[\frac{C_1 \Gamma(l+1-s)\Gamma(1-\bar{Q}+s)}{\Gamma(-l-\bar{Q})} + \frac{C_2 \Gamma(l+1+s)\Gamma(1+\bar{Q}-s)}{\Gamma(-l+\bar{Q})} \right], \quad (\text{A3})$$

where the ratio of the coefficients C_1/C_2 is fixed by the boundary condition at the surface of the ECO.

At infinity, the radial wave equation (3) reduces to [50]

$$r\partial_r^2 f_s + 2(l+1 - i\omega r)\partial_r f_s - 2i(l+1-s)\omega f_s = 0, \quad (\text{A4})$$

where $f_s = e^{i\omega r} r^{-l+s} R_s$. The general solution of Eq. (A4) is a linear combination of a confluent hypergeometric function and a Laguerre polynomial:

$$R_s = e^{-i\omega r} r^{l-s} [C_3 U(l+1-s, 2l+2, 2i\omega r) + C_4 L_{-l-1+s}^{2l+1}(2i\omega r)], \quad (\text{A5})$$

where $C_4 = (-1)^{l-s} C_3 \Gamma(-l+s)$ by imposing only outgoing waves at infinity. The small- r behavior of the solution is

$$R_s \sim C_3 r^{l-s} \frac{(-1)^{l-s} \Gamma(l+1+s)}{2 \Gamma(2l+2)} + C_3 r^{-l-1-s} (2i\omega)^{-(2l+1)} \frac{\Gamma(2l+1)}{\Gamma(l+1-s)}. \quad (\text{A6})$$

The matching of Eqs. (A3) and (A6) in the intermediate region yields

$$\frac{C_1}{C_2} = -\frac{\Gamma(l+1+s)}{\Gamma(l+1-s)} \left[\frac{R_+ + i(-1)^l (\omega(r_+ - r_-))^{2l+1} L S_+}{R_- + i(-1)^l (\omega(r_+ - r_-))^{2l+1} L S_-} \right], \quad (\text{A7})$$

where

$$R_{\pm} \equiv \frac{\Gamma(1 \pm \bar{Q} \mp s)}{\Gamma(l+1 \pm \bar{Q})}, \quad S_{\pm} \equiv \frac{\Gamma(1 \pm \bar{Q} \mp s)}{\Gamma(-l \pm \bar{Q})}, \quad (\text{A8})$$

$$L \equiv \frac{1}{2} \left[\frac{2^l \Gamma(l+1+s) \Gamma(l+1-s)}{\Gamma(2l+1) \Gamma(2l+2)} \right]^2.$$

A. Electromagnetic case

For $s = -1$, the ratio C_1/C_2 is derived by imposing the boundary conditions of Eq. (12) in the near-horizon expansion of the solution in the near-horizon region. At the surface, we obtain

$$\frac{C_1}{C_2} = \mp B^{-1} \bar{Q} x_0^{\bar{Q}}, \quad (\text{A9})$$

where $x_0 = x(r_0)$, and the minus and plus signs refer to polar and axial perturbations, respectively.

By equating Eq. (A7) with Eq. (A9), we obtain an algebraic equation for the complex frequency ω . An approximate solution of ω can be found in the regime $a \ll M$ and $\epsilon \ll 1$, i.e., $\bar{Q} \ll 1$. In this case, Eq. (A7)

reduces to $C_1/C_2 = \bar{Q}/[l(l+1)]$, whereas $B \approx l(l+1)$ in Eq. (A9). It follows that

$$x_0^{-2iQ} = \mp 1. \quad (\text{A10})$$

By using the tortoise coordinate $r_*^0 = r_*(r_0)$, where $\log(x_0) \sim r_*^0(r_+ - r_-)/(r_+^2 + a^2)$, Eq. (A10) yields

$$e^{-2iQ r_*^0(r_+ - r_-)/(r_+^2 + a^2)} = \mp 1, \quad (\text{A11})$$

which is analogous to Eq. (A18) in Ref. [50] for the scalar-field case. The solution of Eq. (A11) is

$$\omega = -\frac{\pi q}{2|r_*^0|} + m\Omega, \quad (\text{A12})$$

where q is a positive odd (even) integer for polar (axial) modes. Equation (A12) is also valid for scalar perturbations where q is a positive odd (even) integer for the modes with Neumann (Dirichlet) boundary conditions on Teukolsky's function.

B. Gravitational case

For $s = -2$, the ratio C_1/C_2 is derived by imposing the boundary conditions of Eq. (14) in the near-horizon expansion of the solution in the near-horizon region. At the surface, when $\bar{Q} \ll 1$, we obtain

$$\frac{C_1}{C_2} = \mp \frac{2}{(l+2)(l+1)l(l-1)} \bar{Q} x_0^{\bar{Q}}, \quad (\text{A13})$$

where the minus and plus signs refer to polar and axial perturbations, respectively. When $\bar{Q} \ll 1$, Eq. (A7) reduces to $C_1/C_2 = -2\bar{Q}/[(l+2)(l+1)l(l-1)]$. By equating the latter equation with Eq. (A13), we get

$$x_0^{-2iQ} = \pm 1, \quad (\text{A14})$$

whose solution is

$$\omega = -\frac{\pi(q+1)}{2|r_*^0|} + m\Omega, \quad (\text{A15})$$

where q is a positive odd (even) integer for polar (axial) modes. We conclude that in the gravitational case, the frequency has an additional phase π with respect to the scalar and electromagnetic case.

APPENDIX B: TRANSFORMATIONS OF TEUKOLSKY'S EQUATION TO A REAL POTENTIAL

In this appendix, we revisit and extend the computation by Detweiler [66] and derive the transformation of

Teukolsky's function to bring Eq. (3) into a form like Eq. (6) with a real potential. In doing so, we correct some mistakes of Ref. [66]. On the other hand, we note that the electromagnetic case presented in Ref. [66] is correct, and we refer the reader to the original work for the explicit transformation.⁷

The Starobinskii identity for gravitational perturbations reads [65]

$$\frac{1}{4}R_2 = \mathcal{D}DDDR_{-2}, \quad (\text{B1})$$

where $\mathcal{D} = \partial_r - iK/\Delta$. According to Eq. (B1), we can write

$$R_2 = \mathbf{a}R_{-2} + \frac{\mathbf{b}}{\Delta} \frac{dR_{-2}}{dr}, \quad (\text{B2})$$

where

$$\mathbf{a} = (a_1 + ia_2), \quad (\text{B3})$$

$$\mathbf{b} = ib_2, \quad (\text{B4})$$

and

$$a_1 = 4 \left[\frac{8K^4}{\Delta^4} + \frac{8K^2}{\Delta^3} \left(\frac{M^2 - a^2}{\Delta} - \lambda \right) - \frac{4\omega K}{\Delta^3} (3r^2 + 2Mr - 5a^2) + \frac{12r^2\omega^2 + \lambda(\lambda + 2)}{\Delta^2} \right], \quad (\text{B5})$$

$$a_2 = 4 \left\{ -\frac{24\omega r K^2}{\Delta^3} + \frac{1}{\Delta^2} \left[\frac{4\lambda(r-M)K}{\Delta} + 4\omega r\lambda + 12\omega M \right] \right\}, \quad (\text{B6})$$

$$b_2 = 4 \left\{ \frac{8K^3}{\Delta^2} + \frac{4K}{\Delta} \left[\frac{2(M^2 - a^2)}{\Delta} - \lambda \right] - \frac{8\omega}{\Delta} (Mr - a^2) \right\}. \quad (\text{B7})$$

The radial functions α and β which define the Detweiler's function in Eq. (5) are

⁷To the best of our knowledge, Ref. [82] reported a misprint in the effective potential, Eq. (B23) of Ref. [66], but did not provide the corresponding expressions for the functions α and β . In this Appendix, we correct several mistakes in Eqs. (B3)–(B14) in Ref. [66] and provide the explicit expressions of α and β , extending the calculations in Ref. [83] to gravitational perturbations.

$$\alpha = \frac{\kappa\mathbf{a}\Delta^2 + |\kappa|^2}{\sqrt{2}|\kappa|(a_1\Delta^2 + \text{Re}\kappa)^{1/2}}, \quad (\text{B8})$$

$$\beta = \frac{i\kappa b_2\Delta^2}{\sqrt{2}|\kappa|(a_1\Delta^2 + \text{Re}\kappa)^{1/2}}, \quad (\text{B9})$$

where

$$\begin{aligned} \kappa = & 4[\lambda^2(\lambda + 2)^2 + 144a^2\omega^2(m - a\omega)^2 \\ & - a^2\omega^2(40\lambda^2 - 48\lambda) + a\omega m(40\lambda^2 + 48\lambda)]^{1/2} \\ & + 48i\omega M, \end{aligned} \quad (\text{B10})$$

$$\begin{aligned} \text{Re}\kappa = & 4[\lambda^2(\lambda + 2)^2 + 144a^2\omega^2(m - a\omega)^2 \\ & - a^2\omega^2(40\lambda^2 - 48\lambda) + a\omega m(40\lambda^2 + 48\lambda)]^{1/2}, \end{aligned} \quad (\text{B11})$$

$$\begin{aligned} |\kappa| = & \{16[\lambda^2(\lambda + 2)^2 + 144a^2\omega^2(m - a\omega)^2 \\ & - a^2\omega^2(40\lambda^2 - 48\lambda) + a\omega m(40\lambda^2 + 48\lambda)] \\ & + (48\omega M)^2\}^{1/2}. \end{aligned} \quad (\text{B12})$$

With this choice of parameters, α and β satisfy the following relation:

$$\alpha^2 - \alpha'\beta\Delta^{s+1} + \alpha\beta'\Delta^{s+1} - \beta^2\Delta^{2s+1}V_s = \kappa, \quad (\text{B13})$$

which guarantees that the Detweiler's function defined in Eq. (5) satisfies Eq. (6). Furthermore, the conserved flux of energy is the same if computed by two independent solutions of Teukolsky's equation [Eq. (3)] or two independent solutions of Detweiler's equation [Eq. (6)] [83]. This is an important consistency check, since the energy flux is a measurable quantity and cannot depend on the transformation of the perturbation variable.

Equation (7) gives the following potential:

$$V(r, \omega) = \frac{-K^2 + \Delta\lambda}{(r^2 + a^2)^2} + \frac{\Delta(b_2 p' \Delta)'}{(r^2 + a^2)^2 b_2 p} + G^2 + \frac{dG}{dr_*}, \quad (\text{B14})$$

where

$$p \equiv |\kappa|[2(a_1\Delta^2 + \text{Re}\kappa)]^{-1/2}. \quad (\text{B15})$$

The effective potential (B14) is purely real and has the following asymptotic forms: $V(r \rightarrow +\infty, \omega) \rightarrow -\omega^2$ and $V(r \rightarrow r_+, \omega) \rightarrow -\tilde{\omega}^2$.

- [1] V. Cardoso, S. Hopper, C. F. B. Macedo, C. Palenzuela, and P. Pani, *Phys. Rev. D* **94**, 084031 (2016).
- [2] V. Cardoso and P. Pani, *Nat. Astron.* **1**, 586 (2017).
- [3] V. Cardoso and P. Pani, arXiv:1707.03021.
- [4] P. Pani and V. Ferrari, *Classical Quantum Gravity* **35**, 15 (2018).
- [5] L. Barack *et al.*, arXiv:1806.05195.
- [6] R. Ruffini and S. Bonazzola, *Phys. Rev.* **187**, 1767 (1969).
- [7] S. L. Liebling and C. Palenzuela, *Living Rev. Relativity* **15**, 6 (2012).
- [8] F. D. Ryan, *Phys. Rev. D* **55**, 6081 (1997).
- [9] P. Pani, *Phys. Rev. D* **92**, 124030 (2015).
- [10] N. Uchikata and S. Yoshida, *Classical Quantum Gravity* **33**, 025005 (2016).
- [11] N. Uchikata, S. Yoshida, and P. Pani, *Phys. Rev. D* **94**, 064015 (2016).
- [12] P. V. P. Cunha, C. A. R. Herdeiro, E. Radu, and H. F. Runarsson, *Phys. Rev. Lett.* **115**, 211102 (2015).
- [13] C. B. M. H. Chirenti and L. Rezzolla, *Classical Quantum Gravity* **24**, 4191 (2007).
- [14] P. Pani, E. Berti, V. Cardoso, Y. Chen, and R. Norte, *Phys. Rev. D* **80**, 124047 (2009).
- [15] C. F. B. Macedo, P. Pani, V. Cardoso, and L. C. B. Crispino, *Phys. Rev. D* **88**, 064046 (2013).
- [16] C. Chirenti and L. Rezzolla, *Phys. Rev. D* **94**, 084016 (2016).
- [17] M. Wade, J. D. E. Creighton, E. Ochsner, and A. B. Nielsen, *Phys. Rev. D* **88**, 083002 (2013).
- [18] V. Cardoso, E. Franzin, and P. Pani, *Phys. Rev. Lett.* **116**, 171101 (2016); *Phys. Rev. Lett.* **117**, 089902(E) (2016).
- [19] N. Sennett, T. Hinderer, J. Steinhoff, A. Buonanno, and S. Ossokine, *Phys. Rev. D* **96**, 024002 (2017).
- [20] P. O. Mazur and E. Mottola, arXiv:gr-qc/0109035.
- [21] S. D. Mathur, *Fortschr. Phys.* **53**, 793 (2005).
- [22] K. Skenderis and M. Taylor, *Phys. Rep.* **467**, 117 (2008).
- [23] A. Almheiri, D. Marolf, J. Polchinski, and J. Sully, *J. High Energy Phys.* **02** (2013) 062.
- [24] S. B. Giddings, *Phys. Rev. D* **90**, 124033 (2014).
- [25] B. Holdom and J. Ren, *Phys. Rev. D* **95**, 084034 (2017).
- [26] R. Brustein, A. J. M. Medved, and K. Yagi, *Phys. Rev. D* **96**, 124021 (2017).
- [27] C. Barceló, R. Carballo-Rubio, and L. J. Garay, *J. High Energy Phys.* **05** (2017) 054.
- [28] M. A. Abramowicz, W. Kluzniak, and J. P. Lasota, *Astron. Astrophys.* **396**, L31 (2002).
- [29] V. Ferrari and K. D. Kokkotas, *Phys. Rev. D* **62**, 107504 (2000).
- [30] J. Abedi, H. Dykaar, and N. Afshordi, *Phys. Rev. D* **96**, 082004 (2017).
- [31] R. S. Conklin, B. Holdom, and J. Ren, *Phys. Rev. D* **98**, 044021 (2018).
- [32] G. Ashton, O. Birnholtz, M. Cabero, C. Capano, T. Dent, B. Krishnan, G. D. Meadors, A. B. Nielsen, A. Nitz, and J. Westerweck, arXiv:1612.05625.
- [33] J. Abedi, H. Dykaar, and N. Afshordi, arXiv:1701.03485.
- [34] J. Westerweck, A. Nielsen, O. Fischer-Birnholtz, M. Cabero, C. Capano, T. Dent, B. Krishnan, G. Meadors, and A. H. Nitz, *Phys. Rev. D* **97**, 124037 (2018).
- [35] J. Abedi, H. Dykaar, and N. Afshordi, arXiv:1803.08565.
- [36] V. Cardoso, E. Franzin, A. Maselli, P. Pani, and G. Raposo, *Phys. Rev. D* **95**, 084014 (2017).
- [37] A. Maselli, P. Pani, V. Cardoso, T. Abdelsalhin, L. Gualtieri, and V. Ferrari, *Phys. Rev. Lett.* **120**, 081101 (2018).
- [38] N. V. Krishnendu, K. G. Arun, and C. K. Mishra, *Phys. Rev. Lett.* **119**, 091101 (2017).
- [39] S. M. Du and Y. Chen, *Phys. Rev. Lett.* **121**, 051105 (2018).
- [40] E. Barausse, R. Brito, V. Cardoso, I. Dvorkin, and P. Pani, *Classical Quantum Gravity* **35**, 20LT01 (2018).
- [41] X. L. Fan and Y. B. Chen, *Phys. Rev. D* **98**, 044020 (2018).
- [42] J. L. Friedman, *Commun. Math. Phys.* **63**, 243 (1978).
- [43] R. Brito, V. Cardoso, and P. Pani, *Lect. Notes Phys.* **906**, 1 (2015).
- [44] R. Penrose, *Nuovo Cimento* **1**, 252 (1969).
- [45] A. Vilenkin, *Phys. Lett.* **78B**, 301 (1978).
- [46] N. Comins and B. F. Schutz, *Proc. R. Soc. A* **364**, 211 (1978).
- [47] S. Yoshida and Y. Eriguchi, *Mon. Not. R. Astron. Soc.* **282**, 580 (1996).
- [48] K. D. Kokkotas, J. Ruoff, and N. Andersson, *Phys. Rev. D* **70**, 043003 (2004).
- [49] V. Cardoso, P. Pani, M. Cadoni, and M. Cavaglia, *Phys. Rev. D* **77**, 124044 (2008).
- [50] V. Cardoso, P. Pani, M. Cadoni, and M. Cavaglia, *Classical Quantum Gravity* **25**, 195010 (2008).
- [51] P. Pani, E. Barausse, E. Berti, and V. Cardoso, *Phys. Rev. D* **82**, 044009 (2010).
- [52] C. B. M. H. Chirenti and L. Rezzolla, *Phys. Rev. D* **78**, 084011 (2008).
- [53] V. Cardoso, L. C. B. Crispino, C. F. B. Macedo, H. Okawa, and P. Pani, *Phys. Rev. D* **90**, 044069 (2014).
- [54] E. Maggio, P. Pani, and V. Ferrari, *Phys. Rev. D* **96**, 104047 (2017).
- [55] R. Vicente, V. Cardoso, and J. C. Lopes, *Phys. Rev. D* **97**, 084032 (2018).
- [56] K. Yagi and N. Yunes, *Phys. Rev. D* **91**, 123008 (2015).
- [57] K. Yagi and N. Yunes, *Phys. Rev. D* **91**, 103003 (2015).
- [58] C. Posada, *Mon. Not. R. Astron. Soc.* **468**, 2128 (2017).
- [59] Z. Mark, A. Zimmerman, S. M. Du, and Y. Chen, *Phys. Rev. D* **96**, 084002 (2017).
- [60] Q. Wang and N. Afshordi, *Phys. Rev. D* **97**, 124044 (2018).
- [61] C. P. Burgess, R. Plestid, and M. Rummel, *J. High Energy Phys.* **09** (2018) 113.
- [62] E. G. Gimon and P. Horava, *Phys. Lett. B* **672**, 299 (2009).
- [63] S. A. Teukolsky, *Phys. Rev. Lett.* **29**, 1114 (1972).
- [64] S. A. Teukolsky, *Astrophys. J.* **185**, 635 (1973).
- [65] S. A. Teukolsky and W. H. Press, *Astrophys. J.* **193**, 443 (1974).
- [66] S. Detweiler, *Proc. R. Soc. A* **352**, 381 (1977).
- [67] A. R. King, *Math. Proc. Cambridge Philos. Soc.* **81**, 149 (1977).
- [68] P. Pani, *Int. J. Mod. Phys. A* **28**, 1340018 (2013).
- [69] E. W. Leaver, *Proc. R. Soc. A* **402**, 285 (1985).
- [70] E. Berti, V. Cardoso, and M. Casals, *Phys. Rev. D* **73**, 024013 (2006).
- [71] M. Casals and A. C. Ottewill, *Phys. Rev. D* **71**, 124016 (2005).

- [72] A. A. Starobinskij and S. M. Churilov, *Zh. Eksp. Teor. Fiz.* **65**, 3 (1973); <http://www.jetp.ac.ru/cgi-bin/e/index/e/38/1/p1?a=list>.
- [73] K. Glampedakis, A. D. Johnson, and D. Kennefick, *Phys. Rev. D* **96**, 024036 (2017).
- [74] S. Chandrasekhar, *The Mathematical Theory of Black Holes* (Oxford University Press, New York, 1983).
- [75] S. Hod, *J. High Energy Phys.* 06 (2017) 132.
- [76] S. Hod, *Phys. Lett. B* **774**, 582 (2017).
- [77] R. H. Price and G. Khanna, *Classical Quantum Gravity* **34**, 225005 (2017).
- [78] B. P. Abbott *et al.* (Virgo and LIGO Scientific Collaboration), *Phys. Rev. Lett.* **116**, 131102 (2016).
- [79] B. P. Abbott *et al.* (Virgo and LIGO Scientific Collaboration), *Phys. Rev. Lett.* **118**, 121101 (2017).
- [80] W. H. Press and S. A. Teukolsky, *Nature (London)* **238**, 211 (1972).
- [81] A. Testa and P. Pani, *Phys. Rev. D* **98**, 044018 (2018).
- [82] E. Seidel and S. Iyer, *Phys. Rev. D* **41**, 374 (1990).
- [83] S. Detweiler, *Proc. R. Soc. London Ser. A* **349**, 217 (1976) ; https://www.jstor.org/stable/79029?seq=1#page_scan_tab_contents.